CHAPTER 4 - Characterization Results

This chapter deals with results of different characterization studies.

4.1 X-ray Diffraction (XRD)

4.1.1 Introduction

X-ray Diffraction (XRD) is a basic tool to characterize the microstructure of a crystalline or polycrystalline material. It is a versatile tool which is extensively used in solid state electrochemistry also. XRD was used to characterize and confirm the microstructure of NASICON compounds synthesized for the current study.

4.1.2 X-ray Diffraction of $LiTi_2(PO_4)_3$ (LTP) system

The structural characterization of the above mentioned LTP, LATP, LAMTP (M = Y, Ga, Sc) for different concentrations is performed using X-ray Diffraction (XRD) technique. Peaks corresponding to $LiTi_2(PO_4)_3$ (LTP) phase are seen at $2\theta \approx 24°$, 30°, 33°, 36°, 47° and 51° indicated by pointers in the Fig.4.1 We also observe some impurity peaks for TiO_2 (TiP_2O_7) type of rutile phases. These phases were identified using the JCPDS catalogue [1, 2] and through cross referencing [3]. The pellets were exposed to a collimated beam of monochromatic x-rays of wavelength ($\lambda = 1.5404$ Å) in a vertical geometry.

The XRD patterns for LATP systems were also carried out and are shown in the Fig.4.1 (next page). The $LiTi_2(PO_4)_3$ phases are formed as a result of rhombohedral arrangement and have a $R\bar{3}c$ space group. Typically the values of lattice parameters corresponding to the rhombohedral structure are in the range of ***a*** = 8.5 Å, ***b*** = 8.5 Å and ***c*** = 20.5 Å [4, 12]. The values of ***a, b, c*** are obtained from Reitveld refinement. Specialized software like SCANIX, TOPAZ and others are generally employed to perform the Reitveld analysis [12, 14, 15, 17]. When trivalent cations like Yttrium, Scandium, Indium, Aluminum etc are doped in to these Lithium based NASICON compounds, the basic structure and arrangement of the $LiTi_2(PO_4)_3$ lattice remains more or less the same due to rigid and stable geometrical structure of the LTP lattice. The structure gets its rigidity from the PO_4 tetrahedrons which are connected to each other by sharing a common oxygen atom [12, 13]. The doping species either replace the tetravalent cations like Ti^{4+} or stay near the LTP structure. These doped atoms also are in way accommodated within the LTP geometry. The

doping of done at the Al and Ti sites in the system. Hence MO_6 octahedrons are responsible for the flexible nature (to allow the doped species) of the LTP lattice. The LTP at low concentrations retains the rhombohedral geometry [12] but as the concentration of the doping species (cations) increases beyond a certain threshold (generally $x > 0.7$), the rhombohedral structure gets distorted as the bonds connecting the MO_6 octahedra with PO_4 tetrahedra is titled along the ***c***-axis [13, 26]. At low doping concentrations, as in our study (where maximum value of $x = 0.15$), the rhombohedral structure obtained even after doping is retained and the doped cations reside near the LTP structure. Due to this, the doped NASICON compounds contain peaks of LTP in their XRD patterns. We see such structures in the XRD patterns of LAYTP, LAGTP and

LASTP series in the below sections.

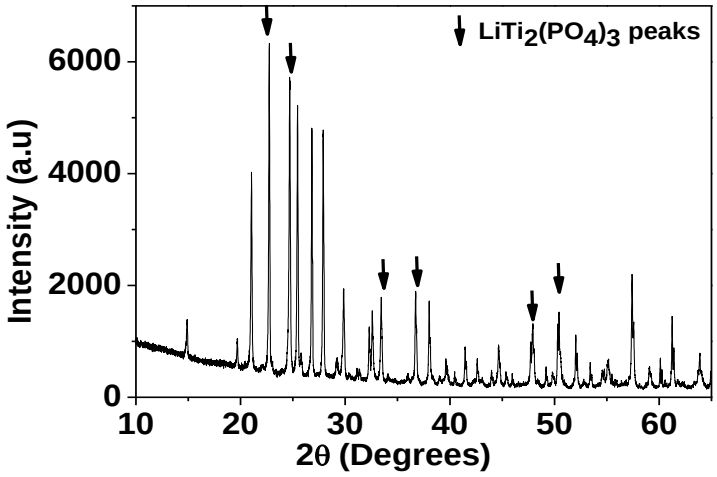

Fig. 4.1 XRD patterns of $LiTi_2(PO_4)_3$ (LTP) system where the LTP peaks are indicated by pointers. The NASICON LTP units have a $R\bar{3}c$ structure.

A brief description of the rhombohedral symmetry of the NASICON compounds and LTP in particular are now given below: The rhombohedral structure is formed as a result of sharing the oxygen atoms at corners of each of the six tetrahedra (PO_4) and two octahedra (MO_6). Chains of alternately placed tetrahedra and octahedra are formed along ***c***-axis while corner oxygen sharing between intra chains tetrahedra along ***a***-axis form the **M1** and **M2** sites.

The rhombohedral structure is formed as a result of chains which are formed of two octahedral (TiO_6) units facing each other. These octahedral units are connected by oxygen atoms of PO_4 tetrahedra. The chains are formed along the **c**-axis. The M1 positions are the gaps between the adjacently facing octahedral units. Thus the M1 sites are formed along the c-axis and within the ribbons. There are infinite such ribbons (chains) parallel to each other within grains of a NASICON compound. They form $LiTi_2(PO_4)_3$ lattice units. Thus the PO_4 tetrahedra connect the octahedral units between the chains. The gaps between each of PO_4 can also accommodate Li^+ as they diffuse about in the 3-D network. These gaps are called the M2 vacancies. Thus M2 vacancies are formed between the chains (intra-chain) [13]. The following diagrams illustrate the NASICON structure and the place of vacancies in which Li^+ diffuse into. The Li^+ reside and jump diffuse into these cation vacancy sites [7, 8, 13].

4.1.3 X-ray Diffraction for LATP sample

From XRD patterns of LATP sample it is observed that there are LTP peaks in the same position as that observed in the LTP patterns. Some impurity phases like TiO_2 and TiP_2O_7 are also seen and marked in the Fig. 4.2. They seem to be from the unmixed TiO_2 powder. The peaks for AlO_4 (tridimite phases) are also seen. According to Wong *et al.*. [11], (on basis of ^{27}Al and ^{31}P MAS NMR results) the $AlPO_4$.

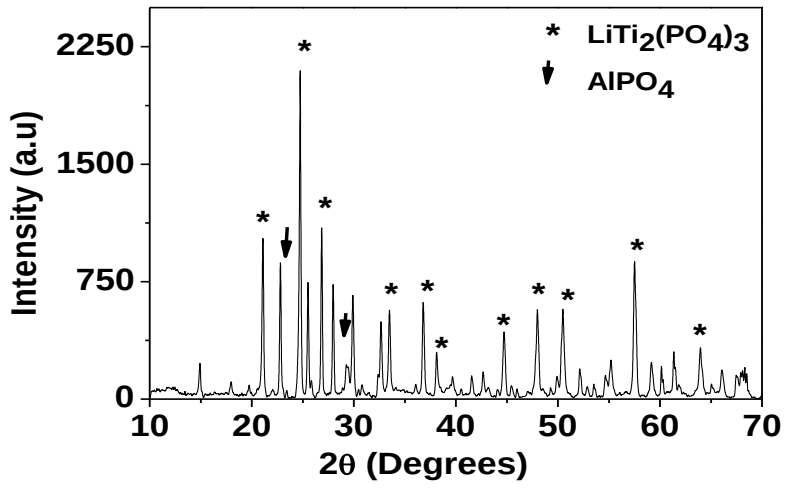

Fig.4.2 XRD patterns of $Li_{1.3}Al_{0.3}Ti_{1.7}(PO_4)_3$ (LATP) system

(Tridimite phases) peaks in a LATP system are formed at 2θ = 21.7° and 35.8° in the XRD patterns by oxygen atoms at corners of $[PO_4]^{3-}$ and $[AlO4]^{5-}$ tetrahedra. In LATP system, the tridimite peaks of this aluminum phase, generally become more intense when Al concentration in the system is more ($x > 0.4$) [4, 5, 8, 12]. These are generally irreversible phases, meaning that once formed the aluminum is locked in these phases and cannot be re-converted into useful phases in LATP and hence cannot be useful for the Li^+ conductivity. Other phases of aluminum formed at higher temperatures are Berlinite and Crystoballite [5, 11]. The phases of aluminum convert into each other as the temperature of the system changes (increases or decreases) [5, 8]. Crystoballite phase is formed at high temperature of 1100° C while the tridimite is formed between 700° C and 1000° C and berlinite is formed before 700° C. Although all the three above mentioned $AlPO_4$ phases are essentially made up of alternating arrangement of tetrahedral lattices of AlO_4 and PO_4, and are chemically similar to each other, they differ from each other in terms of the orientation of AlO_4 and PO_4 tetrahedron. The vacancies formed within the tetrahedron are of different sizes [11]. Therefore essentially, the orientation and size of $AlPO_4$ change with temperature. In our system, the maximum temperature achieved is 1000° C. Hence, tridimite phase of aluminum is the most likely one formed in our system and which is detected in the XRD patterns [9, 10, 11]. The aluminum locked in these phases (especially AlO_4) can never be retrieved back into the system even on heating at extreme temperatures. The $AlPO_4$ phases are generally insulating in nature. $AlPO_4$ phases are segregated towards grain boundary. In the present study, aluminum is already inserted in the system as one of the forming members and at an optimum proportion (concentration $x = 0.3$) to form a system $Li_{1.3}Al_{0.3}Ti_{1.7}(PO_4)_3$ (LATP) system. This system has a maximum conductivity of ~ 10^{-3} S/cm at room temperature. This Li^+ conductivity is one of the highest among the Lithium based NASICON compounds [4, 12]. That is, at the concentration ($x = 0.3$), the system has maximum enlargement of the bottleneck due to tilting of the P-O(1)-Al bond [28]. Besides this, the **M1, M2** vacancy sites are influenced by the proximity of Al^{3+} at the octahedral site. Hence Li^+ have maximum mobility at this site. Other phases formed are $LiAlO_5$ and $AlPO_4$ and denoted by symbols in

XRD patterns. These phases are generally formed when the concentration of Aluminum is higher than $x = 0.4$ in the system [5, 12].

The present system consists of an optimum concentration of aluminum which opens up the bottlenecks for the Li^+ ions to pass through. The presence of doped cation of similar oxidation state (+3) but with larger ionic radii than Al^{3+} will encourage more distortion of the rhombohedral lattice cell of $LiTi_2(PO_4)_3$. Thus the XRD peaks corresponding to LTP phase also get split and shift towards lower 2θ angles. There are impurity phases near the LTP peaks which distort and split the regular LTP peaks in the XRD spectra.

The $Li_{1.3}Al_{0.3}Ti_{1.7}(PO_4)_3$ (LATP) system is formed when trivalent cation Al^{3+} is doped in the $LiTi_2(PO_4)_3$ (LTP) structure. In this case, Al^{3+} (0.53 Å) has a comparable radius to Ti^{4+} (0.60 Å). Hence Al^{3+} is likely to take the place of Ti^{4+} in the LTP structure. That is, Al^{3+} forms bonds with $[PO_4]^{3-}$ tetrahedrons. When it is near PO_4 tetrahedra, it tries to replace P which has an oxidation state of +5 (that is, P^{5+}), and is known as $\mathbf{Al_T}$ and when near MO_6 octahedra it known as $\mathbf{Al_O}$. NMR studies of ^{27}Al cations have concluded that most of the Al^{3+} is deposited at octahedral sites near the Ti^{4+} cations. The ratio of aluminum at tetrahedral and octahedral sites in a LATP system is generally observed to be as $Al_T / Al_O < 0.3$ [10, 11]. On increasing the concentration of Al in the LTP system, the number of Al at tetrahedral sites does not increase in proportion to Al at octahedral sites. [11]. Generally Al at tetrahedral sites function to broaden the M1 – M2 bottleneck. From the Fig. 4.2, it can be noticed that apart from the LTP peaks there are $AlPO_4$ and TiO_2 peaks as well. These peaks correspond to the typical impurities observed in LATP system. The impurities are observed in the grain and grain boundary regions. These points are further discussed in detail in below sections.

4.1.4 X-ray Diffraction for LAYTP series

For the samples of $Li_{1.3}Al_{0.3-x}Y_xTi_{1.7}(PO_4)_3$ (where, x = 0.01, 0.03, 0.05, 0.07, 0.10, 0.15) system, the XRD patterns are given in the below Fig. 4.3. X-rays of wavelength of 1.54 Å were incident on the ceramic pellet in the XRD study. The range of scan was 10° to 70° in the XRD study. In the below table 4.1, the nomenclature of the samples is given for easy

reference. From the XRD patterns obtained it was deduced that the reflections corresponding to $LiTi_2(PO_4)_3$ NASICON phase had a $R\bar{3}c$ structure [14, 15, 16, 17, 18]. Peaks corresponding to impurities like the rutile phases TiO_2, TiP_2O_7 [1, 2] are also marked in the XRD patterns in Fig.4.3.

Table 4.1.1
Samples of $Li_{1.3}Al_{0.3-x}Y_xTi_{1.7}(PO_4)_3$ series for x = 0.01, 0.03, 0.05, 0.07, 0.10 and 0.15

Sample Name	Sample Composition
S1	$Li_{1.3}Al_{0.29}Y_{0.01}Ti_{1.7}(PO_4)_3$
S2	$Li_{1.3}Al_{0.27}Y_{0.03}Ti_{1.7}(PO_4)_3$
S3	$Li_{1.3}Al_{0.25}Y_{0.05}Ti_{1.7}(PO_4)_3$
S4	$Li_{1.3}Al_{0.23}Y_{0.07}Ti_{1.7}(PO_4)_3$
S5	$Li_{1.3}Al_{0.20}Y_{0.10}Ti_{1.7}(PO_4)_3$
S6	$Li_{1.3}Al_{0.15}Y_{0.15}Ti_{1.7}(PO_4)_3$

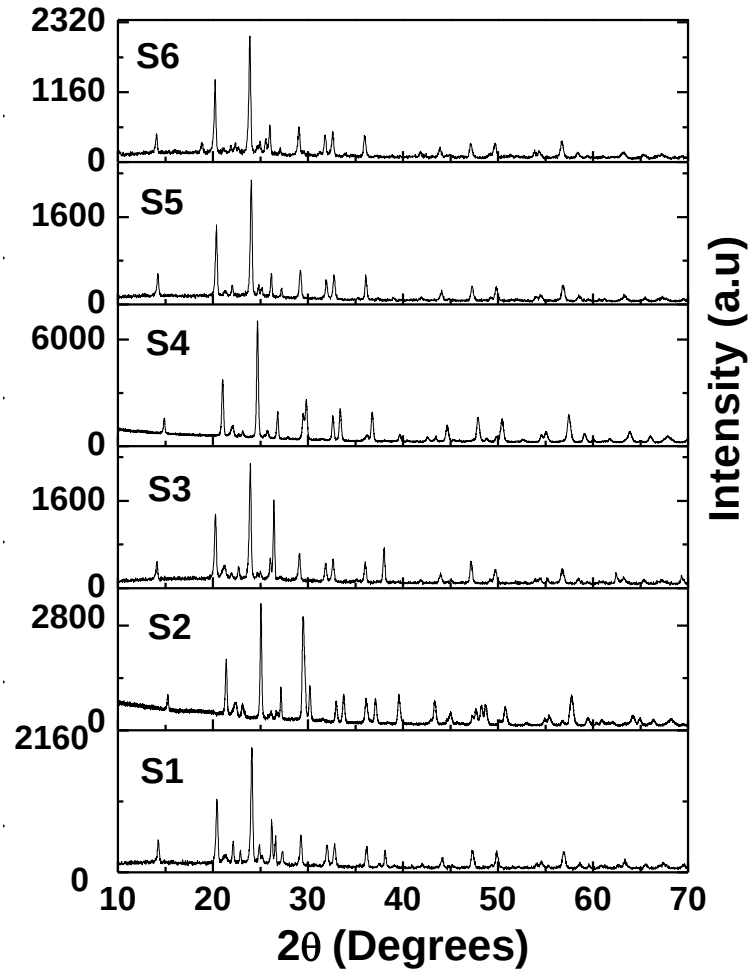

Fig.4.3 XRD patterns of $Li_{1.3}Al_{0.3-x}Y_xTi_{1.7}(PO_4)_3$ (LAYTP) system for x = 0.01, 0.03, 0.05, 0.07, 0.10 and 0.15

The LTP peaks for the rhombohedral phase can be observed at 2θ ~ 24°, 30°, 33°, 36°, 47°. Other phases like AlO_4, $AlPO_4$ are also formed in LATP system [5]. In the Fig.4.3 we observe $AlPO_4$ peaks for $Li_{1.3}Al_{0.3-x}Y_xTi_{1.7}(PO_4)_3$ (where, x = 0.01, 0.03, 0.05, 0.07, 0.10, 0.15) (LAYTP) series. From the XRD patterns it is clear that with decrease in the amount of Al in the system, the intensity of NASICON phase $LiTi_2(PO_4)_3$ peaks typically at 2θ ≈ 24° decreases for samples. Besides, as aluminum decreases the yttrium correspondingly increases in the system. YPO_4 peaks are clearly seen in samples S5 (x = 0.10) and S6 (x = 0.15). Most of the peaks have been identified in the below XRD patterns of LAYTP series. These phases are formed when Y replaces Al at PO_4 sites. These phases affect the grain boundary structure and properties as discussed in later sections.

4.1.5 X-ray Diffraction Studies of LAYTP Heat Treated samples

After the samples were prepared with aforementioned procedure two of the samples of LAYTP series (x = 0.01 and 0.15) were heat treated for 2 and 3 hrs each. The nomenclature details are presented in the table 4.1.2 below.

Table 4.1.2
Samples of $Li_{1.3}Al_{0.3-x}Y_xTi_{1.7}(PO_4)_3$ Series for x = 0.01 and 0.15

Sample Name	Sample Composition	Method of preparation
S1-H2	$Li_{1.3}Al_{0.29}Y_{0.01}Ti_{1.7}(PO_4)_3$	S1 heat treated for 2 hr
S1-H3	$Li_{1.3}Al_{0.29}Y_{0.01}Ti_{1.7}(PO_4)_3$	S1 heat treated for 3 hr
S6-H2	$Li_{1.3}Al_{0.15}Y_{0.15}Ti_{1.7}(PO_4)_3$	S6 heat treated for 2 hr
S6-H3	$Li_{1.3}Al_{0.15}Y_{0.15}Ti_{1.7}(PO_4)_3$	S6 heat treated for 3 hr

The XRD patterns for the samples sintered for 2 hours are presented in Figs. 4.4 and that sintered for 3 hours in Fig. 4.5. The peaks corresponding to LTP, $AlPO_4$, TiO_2, YPO_4 phases are denoted by appropriate symbols. Besides, small peaks corresponding to phases like $LiTiPO_5$ have also been identified in the two Figs. They are formed due to alteration of the LTP structure and movement of Ti which was replaced by Y, towards the grain boundary. These phases are likely formed at grain boundaries [22-25]. According to Key *et al.* [33], the

$AlPO_4$ (Tridimite) phases are impurities and formed in solid state reaction. They have estimated that approximately 10% of material is used in $AlPO_4$ like phases while another 10% in TiO_2 like Rutile phases. Accordingly these phases do not contribute directly towards enhancing the Li^+ conductivity in LATP like systems [24]. The $AlPO_4$ thus formed contributes towards escalating the density of the network [4, 30]. These impurities act to hinder the motion of Li^+ and make the conduction pathways constricted [24]. This is one of the most important reasons of low conductivity of Li^+ at grain boundaries. At times phases like TiO_2 are formed within the grain and block the bottlenecks and decrease the Li^+ conductivity. But due to their minute proportions (as observed from the small peaks) their total contribution to the Li^+ conductivity must be less.

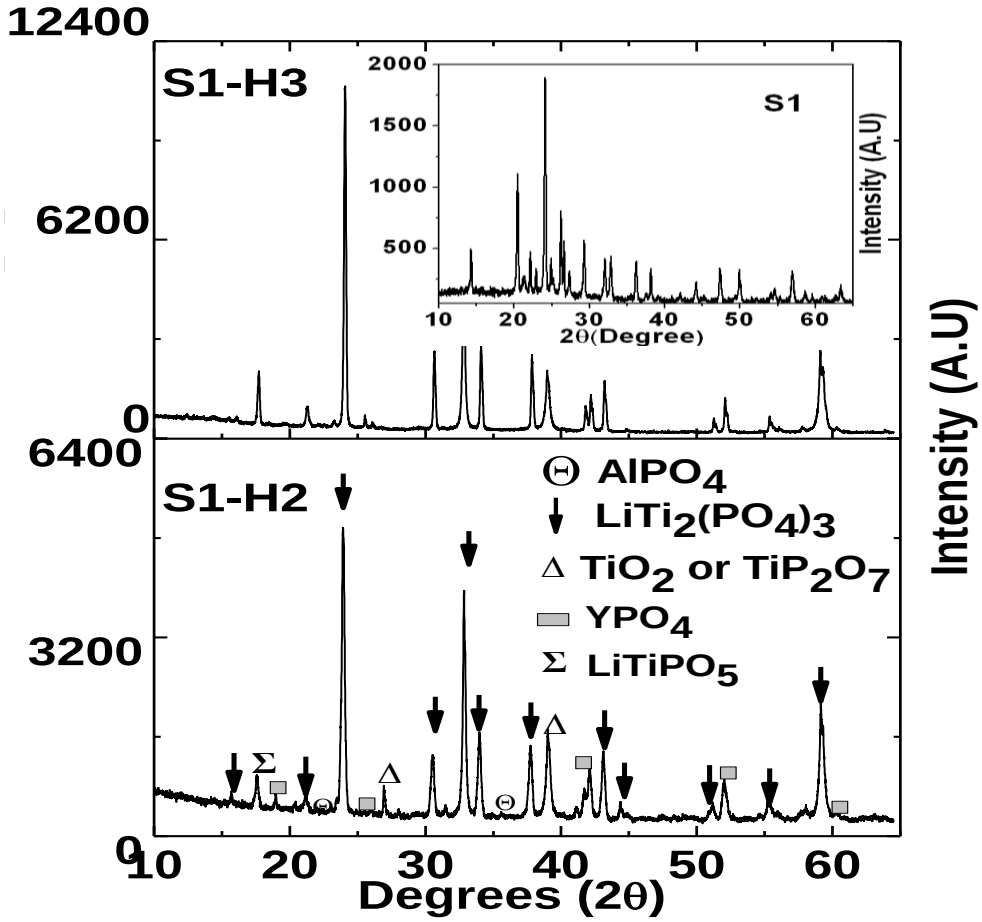

Fig.4.4 XRD patterns of S1-H2 and S1-H3 samples of $Li_{1.3}Al_{0.3-x}Y_xTi_{1.7}(PO_4)_3$ (Inset: Sample prepared with normal procedure.)

In heat treated samples the small peaks either merge into larger ones or become intense. This is typically seen in many studies [6] as also in our case. This is because, the heat treatment alters the local micro structure. The effect of segregation of yttrium towards grain boundary is assisted by high temperatures (1100° C) as yttrium like heavy cations drift towards grain boundary [26]. Fig. 4.5 shows the XRD scans of the samples S1 and S6 (for both – normal and heat treated) of the LAYTP series.

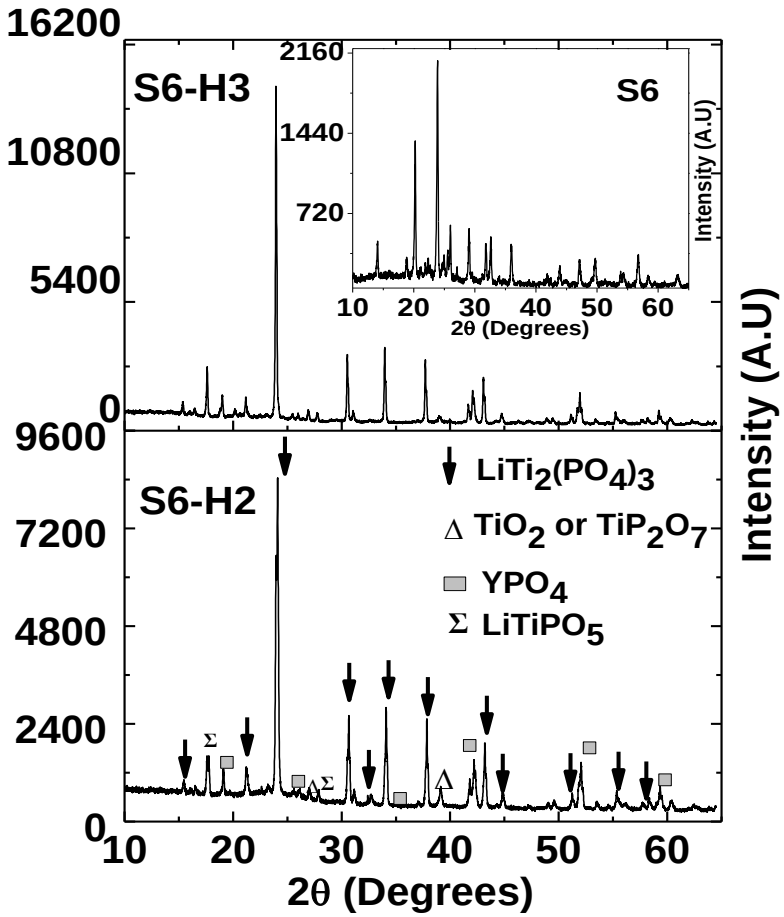

Fig. 4.5 XRD patterns of S6-H2 and S6-H3 samples of $Li_{1.3}Al_{0.3-x}Y_xTi_{1.7}(PO_4)_3$ system Inset: Sample prepared with normal procedure.

NASICON phase ($LiTi_2(PO_4)_3$) peak are prominent and highlighted appropriately in the Figs. 4.4 and 4.5. In these Figures, it is seen that the LTP peaks shift towards left side that is the diffraction angle decreases for these peaks, which indicates an increase in the d-spacing. The d-spacing increases when Y replaces Al in the LTP structure.

Due to this the LTP structure gets distorted and owing to the large size of Y in the lattice, the volume of unit cell increases. This increases the interlayer (**d**) spacing. Small amounts of impurity phases like $AlPO_4$ (tridimite), TiO_2 (or TiP_2O_7) rutile phases, YPO_4 and $LiTiPO_5$ [14] are also noticed in XRD patterns and are indicated by symbols. It can be observed that the intensity of YPO_4 peaks increases with Yttrium content in the system.

4.1.6 X-ray Diffraction Studies of LAGTP Series

Trivalent cation gallium is doped in the LATP system to form $Li_{1.3}Al_{0.3-x}Ga_xTi_{1.7}(PO_4)_3$ (where x = 0.01, 0.03, 0.05, 0.07) (LAGTP) system. In LAGTP series, phases of $GaPO_4$ [19, 20, 21] were detected. The intensity of the peak can indicate the amount of gallium phases segregated in the system under study. The nomenclature of the samples are given in the below table 4.1.3.

Table 4.1.3:
Samples of $Li_{1.3}Al_{0.3-x}Ga_xTi_{1.7}(PO_4)_3$ series for x = 0.01, 0.03, 0.05, 0.07

Sample Name	Sample Composition
G1	$Li_{1.3}Al_{0.29}Ga_{0.01}Ti_{1.7}(PO_4)_3$
G2	$Li_{1.3}Al_{0.27}Ga_{0.03}Ti_{1.7}(PO_4)_3$
G3	$Li_{1.3}Al_{0.25}Ga_{0.05}Ti_{1.7}(PO_4)_3$
G4	$Li_{1.3}Al_{0.23}Ga_{0.07}Ti_{1.7}(PO_4)_3$

The XRD patterns recorded for the $Li_{1.3}Al_{0.3-x}Ga_xTi_{1.7}(PO_4)_3$ (LAGTP) system are presented in the Fig. 4.6 below. The parent $LiTi_2(PO_4)_3$ (LTP) phases with space group ($R\bar{3}c$) is prominently seen at $2\theta \approx 24°$ [4, 5, 6, 16] are marked in the XRD patterns of Fig.4.6.

The parent $LiTi_2(PO_4)_3$ (LTP) phases with space group ($R\bar{3}c$) is prominently seen at $2\theta \approx 24°$ [4, 5, 6, 16] are marked in the XRD patterns of Fig.4.6. All the

systems in the present study are derived from the LTP system. It may be noted that there are a number of phases like $GaPO_4$ and TiO_2 in the XRD patterns. These phases are formed near the grain boundary. When Ga^{3+} tries to replace Al^{3+}, either at Al_T

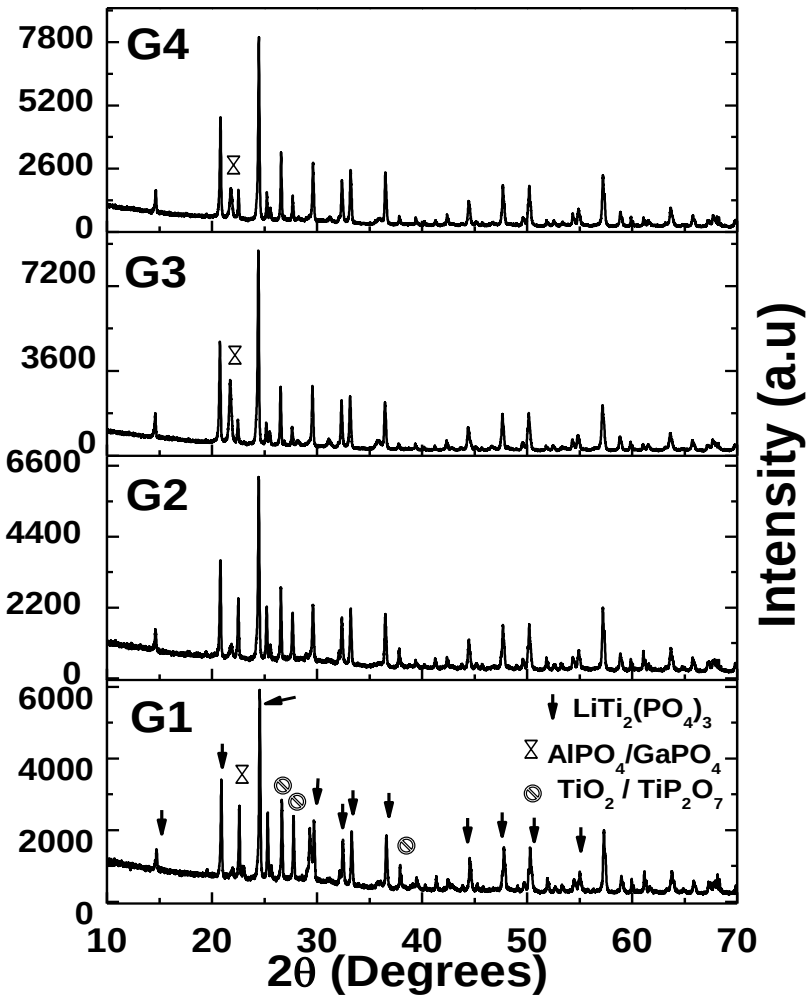

Fig. 4.6 XRD patterns of $Li_{1.3}Al_{0.3-x}Ga_xTi_{1.7}(PO_4)_3$ LAGTP series where x = 0.01, 0.03, 0.05, 0.07

(tetrahedral) or Al_O (octahedral) sites, or Ti^{4+} $GaPO_4$ phases are formed as a result of the replacement.

These phases are found near grain boundary along with $AlPO_4$. Peaks corresponding to $GaPO_4$ [14, 15] or $AlPO_4$ [17] and rutile phases TiO_2 and TiP_2O_7 are

indicated in Fig.4.6. The LTP peaks at 2θ ≈ 24° becomes more intense as gallium concentration in the system increases.

The XRD peaks corresponding to LTP phases at 2θ ≈ 24°, 30°, 36°, 47.5º and 50.5º indicated by arrows, shifts towards lower values of 2θ as the gallium content in the system is increases from samples G1 to G4. The shift is observed when the LTP peaks are compared to LTP and LATP XRD patterns. The peak shift happens, when Ga^{3+} substitutes Al^{3+} in the LATP structure and the unit cell is likely to elongate along ***c***-direction due to larger ionic radii of Ga^{3+} (0.62 Å) compared to Al^{3+} (0.53 Å) [6, 7, 18]. Hence the volume of unit cell increases. Therefore the **d**-spacing increases and results in shifting of peak towards lower values of 2θ.

From the XRD patterns, the peaks corresponding to LTP phase become more intense with increasing gallium content. We also observe $GaPO_4$ or $AlPO_4$ phases in the XRD patterns especially for G3 and G4 and are indicated by a (⧖) symbol.

We observe a slight broadening of the peaks corresponding to LTP phase at 2θ ≈ 24º, 36º, and 50.5º broadens as the gallium content increases of XRD patterns of samples G3 and G4. This indicates a presence of chemical heterogeneities which can be possibly TiO_2 or $GaPO_4$ phases near the LTP sites. We also observe small peaks of rutile phases (TiO_2 and TiP_2O_7) in XRD patterns of G1 sample in Fig 4.6.

4.1.7 X-ray Diffraction Studies of LASTP series

Trivalent cation scandium when doped in LATP system gives $Li_{1.3}Al_{0.3-x}Sc_xTi_{1.7}(PO_4)_3$ (where x = 0.01, 0.03, 0.05, 0.07) (LASTP) system. The below table 4.1.4 gives the details of the nomenclature of the samples.

Table 4.1.4

Samples of Li $_{1.3}Al_{0.3-x}Sc_xTi_{1.7}(PO_4)_3$ series for x = 0.01, 0.03, 0.05, 0.07

Sample Name	Sample Composition
N1	$Li_{1.3}Al_{0.29}Sc_{0.01}Ti_{1.7}(PO_4)_3$
N2	$Li_{1.3}Al_{0.27}Sc_{0.03}Ti_{1.7}(PO_4)_3$
N3	$Li_{1.3}Al_{0.25}Sc_{0.05}Ti_{1.7}(PO_4)_3$
N4	$Li_{1.3}Al_{0.23}Sc_{0.07}Ti_{1.7}(PO_4)_3$

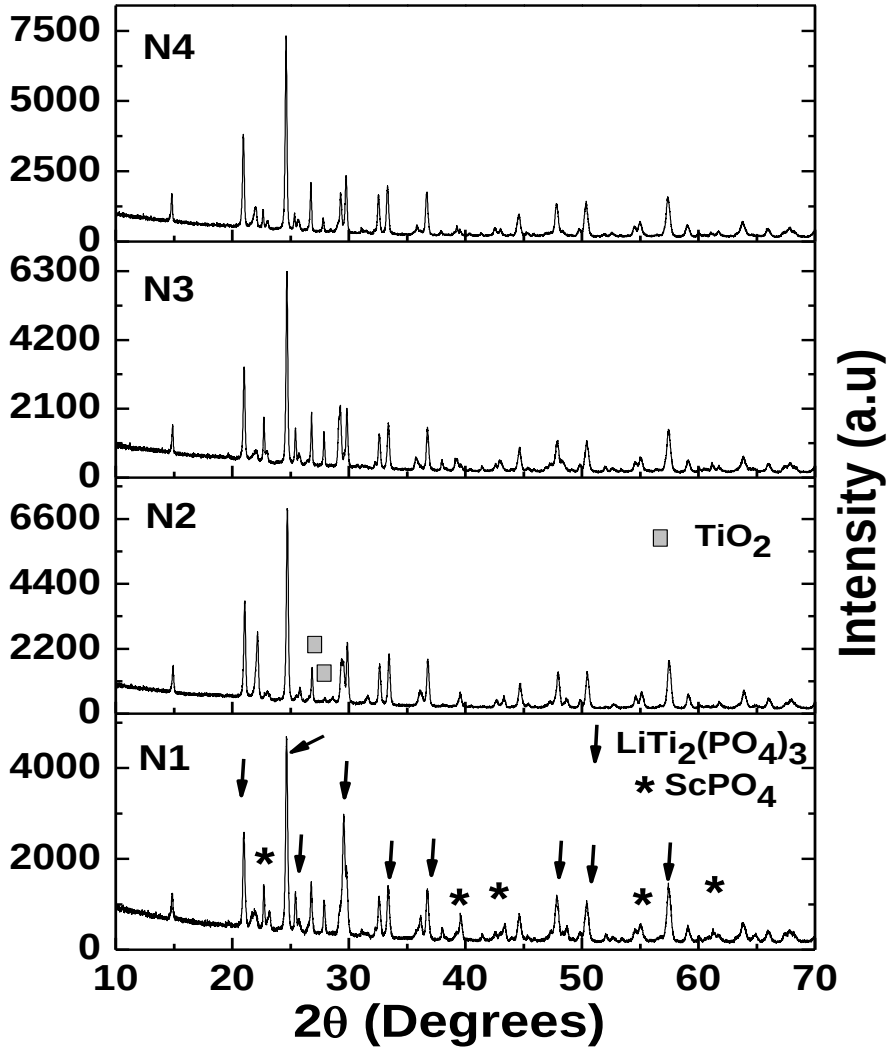

Fig.4.7 XRD patterns of $Li_{1.3}Al_{0.3-x}Sc_xTi_{1.7}(PO_4)_3$ LASTP series where x = 0.01, 0.03, 0.05, 0.07

Fig. 4.7 above shows the XRD patterns of samples of LASTP series. There are a number of phases apart from LTP phase. Some phases of scandium are also present in the XRD patterns. These peaks correspond to the $ScPO_4$ phase [27]. The impurity peaks are less number in the LASTP system compared to LAGTP and LAYTP series. The scandium (0.745 Å) has an oxidation state of +3 and a comparable radius to Ti^{4+} (0.60 Å). The scandium is less likely to replace Al^{3+}, although of same oxidation state due to large difference in the ionic radii. The Sc has octahedral valence shell electrons. These shells are very large compared to Al^{3+} but can easily interact with Ti^{4+} and replaces Ti. The Ti segregates towards grain boundary to form rutile phases like TiO_2 or TiP_2O_7 which try to alter the grain boundary structure and hindering the already constricted pathways of Li^+. This situation arises when amount of Sc^{3+} in the system is high (x = 0.07). Besides this, we also observe a slight shift of peaks towards left side (that is lower values of diffraction angles. This is attributed to larger size of Sc which replaces Al or Ti in the LTP network and increases the lattice cell volume [26].

4.2 Density Measurement

The density measurements were done using the Archimedes principle. The weighing of samples in Methanol and in air was done using a very sensitive weighing balance as described in the previous section.

4.2.1 Density of $LiTi_2(PO_4)_3$ (LTP) and $Li_{1.3}Al_{0.3}Ti_{1.7}(PO_4)_3$ (LATP) system

The density of the reference samples $LiTi_2(PO_4)_3$ (LTP) and $Li_{1.3}Al_{0.3}Ti_{1.7}(PO_4)_3$ (LATP) and for each sample of the series are presented in the following. The LATP sample is denser compared to LTP because of the presence of aluminum. Presence of phases like $AlPO_4$ in the compound also contributes to enhancing the density at the grain boundaries.

Table 4.2.1
Density of $LiTi_2(PO_4)_3$ (LTP) and $Li_{1.3}Al_{0.3}Ti_{1.7}(PO_4)_3$ (LATP) samples.

Sample Name	Sample Composition	Density (g/cm^3)
LTP	$LiTi_2(PO_4)_3$	2.18
LATP	$Li_{1.3}Al_{0.3}Ti_{1.7}(PO_4)_3$	2.24

4.2.2 Density of $Li_{1.3}Al_{0.3-x}Y_xTi_{1.7}(PO_4)_3$ (LAYTP) samples

The density values of the samples of LAYTP series are given in the below table 4.2.2. It is clear that the density of samples of LAYTP series, increase with the amount of massive cations (yttrium) increase in the system. The density also increases because of better contacts at the interfaces of grains due to presence of YPO_4 phase hitherto detected in the XRD patterns also. This is further discussed in the text.

Table 4.2.2
Density of $Li_{1.3}Al_{0.3-x}Y_xTi_{1.7}(PO_4)_3$ (LAYTP) system for x = 0.01, 0.03, 0.05, 0.07, 0.10, 0.15

Sample Name	Sample Composition	Density (g/cm^3)
S1	$Li_{1.3}Al_{0.29}Y_{0.01}Ti_{1.7}(PO_4)_3$	2.28
S2	$Li_{1.3}Al_{0.27}Y_{0.03}Ti_{1.7}(PO_4)_3$	2.31
S3	$Li_{1.3}Al_{0.25}Y_{0.05}Ti_{1.7}(PO_4)_3$	2.35
S4	$Li_{1.3}Al_{0.23}Y_{0.07}Ti_{1.7}(PO_4)_3$	2.39
S5	$Li_{1.3}Al_{0.20}Y_{0.10}Ti_{1.7}(PO_4)_3$	2.41
S6	$Li_{1.3}Al_{0.15}Y_{0.15}Ti_{1.7}(PO_4)_3$	2.45

4.2.3 Density of Heat Treated $Li_{1.3}Al_{0.3-x}Y_xTi_{1.7}(PO_4)_3$ (LAYTP) samples

The density can be enhanced in two ways (1) Either increase the mass of the constituent [4] or (2) decrease the volume by pelletizing the powders. When the pellets are formed at high enough pressures (5 Tons per square inch) the air between the grains of the powders is removed and dense pellets are obtained.

Besides, heat treatment (known as sintering when heat treatment is carried out for 10 hrs or more) is also a used to enhance the density of material by altering the microstructure and fusing of the grains together [6, 31, 32]. Due to heat treatment, the microscopic gaps between grains are reduced as the grain structure is modified. Heat is felt most at the surface of the grains. Two scenarios occur in this situation. (i) A larger number of small grains experience more heat compared to larger grains. Smaller grains, which lie near to each other aggregate to form larger grains. (ii) The smaller grains due to heat experienced at their surface

tend to aggregate into the larger grains. As a result of both the scenarios the free volume between the grains decreases, resulting into a densely packed structure at micro level.

Yttrium is a heavy (rare earth) (atomic mass: 88.906 amu) element which is doped in the LATP system to substitute the light weight aluminum (atomic mass: 26.962 amu) in the LATP lattice. On cold pressing the sample powder at high pressure (pelletizing), it minimizes the physical volume of the material by pushing out the air between the grains of the sample. This reduces the porosity and enhances the volume of the samples. Furthermore, the samples are heat treated to observe the effect on density. Some workers have used hot pressing [27, 29] to enhance the density and decrease the porosity of the samples. In this method, the die in which the pellets are pressed is subjected to higher temperatures to ensure better close packing of the grains.

Commonly used method however is (as in our case), cold pressing in a die set using a hydraulic pelletizer and then subjecting the pellets to high enough temperatures for sufficient durations of time [30]. The samples of LAYTP were prepared by normal method. The samples of the same series at two concentrations (x = 0.01 and x = 0.15) were heat treated for time 2 and 3 hours durations, the density of the samples varied as shown in Table 4.2.3.

Table 4.2.3
Density of Heat treated samples of $Li_{1.3}Al_{0.3-x}Y_xTi_{1.7}(PO_4)_3$ for x = 0.01 and 0.15

Sample Name	Sample Composition	Method of preparation	Density (g/cm^3)
S1	$Li_{1.3}Al_{0.29}Y_{0.01}Ti_{1.7}(PO_4)_3$	S1 as-prepared	2.28
S6	$Li_{1.3}Al_{0.15}Y_{0.15}Ti_{1.7}(PO_4)_3$	S6 as-prepared	2.45
S1-H2	$Li_{1.3}Al_{0.29}Y_{0.01}Ti_{1.7}(PO_4)_3$	S1 heat treated for 2 hr	2.41
S1-H3	$Li_{1.3}Al_{0.29}Y_{0.01}Ti_{1.7}(PO_4)_3$	S1 heat treated for 3 hr	2.46
S6-H2	$Li_{1.3}Al_{0.15}Y_{0.15}Ti_{1.7}(PO_4)_3$	S6 heat treated for 2 hr	2.49
S6-H3	$Li_{1.3}Al_{0.15}Y_{0.15}Ti_{1.7}(PO_4)_3$	S6 heat treated for 3 hr	2.50

Therefore, there was an increase of 6% and 8% in density when the sample S1 (x = 0.01) of same concentration were sintered (heat treated) for 2 and 3 hrs respectively. But corresponding increase was not noted when the sample containing higher concentration of yttrium was subject to heat treatment for the same duration of times (viz. 2and 3 hours). There

was roughly an increase of 1.63% and 2.04% compared to un-sintered (normal) sample. The density of the samples formed also depends on the method of preparation. In one of the studies [15] instead of hand grinding (as in our case), ball milling was performed for 8 hr, 12 hr and 24 hr in 3 different steps. Planetary ball milling was used for these steps. Due to this method, the density was reported to 2.998 g/cm^3 in that study for $Li_{1.3}Al_{0.15}Y_{0.15}Ti_{1.7}(PO_4)_3$ system, while that for $LiTi_2(PO_4)_3$ was 2.948 g/cm^3 and that for $Li_{1.3}Al_{0.3}Ti_{1.7}(PO_4)_3$ (LATP) system was 2.928 g/cm^3. Obviously the planetary ball milling reduced the constituent powders to minute particles of micron size which made mixing and increased the reaction surface area between the particles. This enhanced their bonding and reduced the porosity of the sample.

The density of the samples also increases through an indirect method. When the cations with large cationic radii (like yttrium, as in our case) were doped beyond a certain concentration, they segregated towards grain boundaries and formed glassy phases. Due to this, the mutual contacts between the grains increased and enhanced the overall density of the samples. When such samples are subjected to heat treatment these glassy or semi crystalline phases at grain boundary again get modified and allow better (broader) passage of Li^+. This method to enhance the density was not intended in our study all the same it came as an outcome in our study. Apart from this, we have used all three methods – that is, replaced lighter cations with heavier ones, heat treated some samples, pelletized the samples, and also obtained glassy phases within the structure which also enhanced the density of the materials, in our study.

4.2.4 Density of $Li_{1.3}Al_{0.3-x}Ga_xTi_{1.7}(PO_4)_3$ LAGTP system

The samples of other series mentioned below were also prepared. In the second series, gallium was used to replace the aluminum keeping all other elements constant. $Li_{1.3}Al_{0.3-x}Ga_xTi_{1.7}(PO_4)_3$ for $x = 0.01, 0.03, 0.05, 0.07$.

The results of density of the samples of a series, in which the aluminum is replaced with Gallium was found to increase (Table 4.2.4). Gallium phases like $GaPO_4$ were found to

get segregated at grain boundary and alter its structure there. This also contributed marginally to enhance the density of the samples in this series.

Table 4.2.4

Density of $Li_{1.3}Al_{0.3-x}Ga_xTi_{1.7}(PO_4)_3$ series for x = 0.01, 0.03, 0.05, 0.07

Sample Name	Sample Composition	Density (g/cm^3)
G1	$Li_{1.3}Al_{0.29}Ga_{0.01}Ti_{1.7}(PO_4)_3$	2.45
G2	$Li_{1.3}Al_{0.27}Ga_{0.03}Ti_{1.7}(PO_4)_3$	2.48
G3	$Li_{1.3}Al_{0.25}Ga_{0.05}Ti_{1.7}(PO_4)_3$	2.52
G4	$Li_{1.3}Al_{0.23}Ga_{0.07}Ti_{1.7}(PO_4)_3$	2.56

4.2.5 Density of $Li_{1.3}Al_{0.3-x}Sc_xTi_{1.7}(PO_4)_3$ (LASTP) system

Scandium which is a transition element was doped to replace trivalent Aluminum in the above series. Four samples of this series were prepared. The effect on density, due to this kind of doping was measured. The density results for scandium doped samples are given in Table 4.2.5.

Table 4.2.5

Density of samples of $Li_{1.3}Al_{0.3-x}Sc_xTi_{1.7}(PO_4)_3$ series for x=0.01,0.03,0.05,0.07

Sample Name	Sample Composition	Density (g/cm^3)
N1	$Li_{1.3}Al_{0.29}Sc_{0.01}Ti_{1.7}(PO_4)_3$	3.1975
N2	$Li_{1.3}Al_{0.27}Sc_{0.03}Ti_{1.7}(PO_4)_3$	3.1077
N3	$Li_{1.3}Al_{0.25}Sc_{0.05}Ti_{1.7}(PO_4)_3$	3.1603
N4	$Li_{1.3}Al_{0.23}Sc_{0.07}Ti_{1.7}(PO_4)_3$	3.2221

4.3 Scanning Electron Microscopy (SEM) Studies

The Scanning electron microscopy was performed on samples of different series to investigate the surface morphology and characteristics. The results are presented here below.

4.3.1 SEM of samples of LAYTP series

The SEM pictures of samples of LAYTP series are presented below. All the samples were polished. The SEM pictures were captured at different magnifications. The surface morphology and characteristics changes observed with variation in the concentration are noted in the below Figs 4.8 to 4.11.

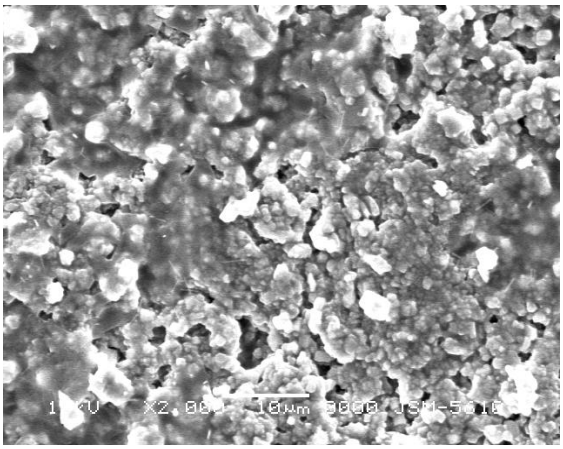

Fig. 4.8 SEM of $Li_{1.3}Al_{0.3}Y_{0.3-x}Ti_{1.7}(PO_4)_3$ for x= 0.01 sample at 2000X magnification

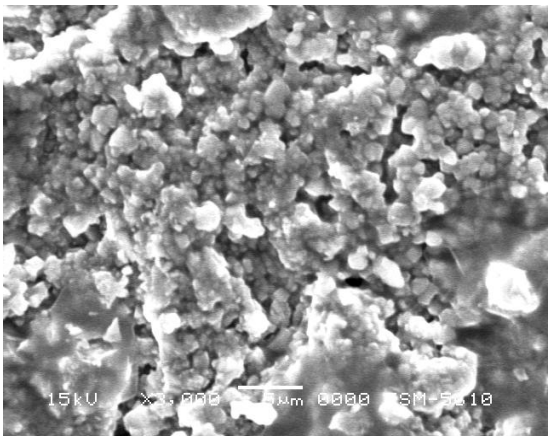

Fig. 4.9 SEM of $Li_{1.3}Al_{0.3}Y_{0.3-x}Ti_{1.7}(PO_4)_3$ for x= 0.01 sample at 3000X magnification

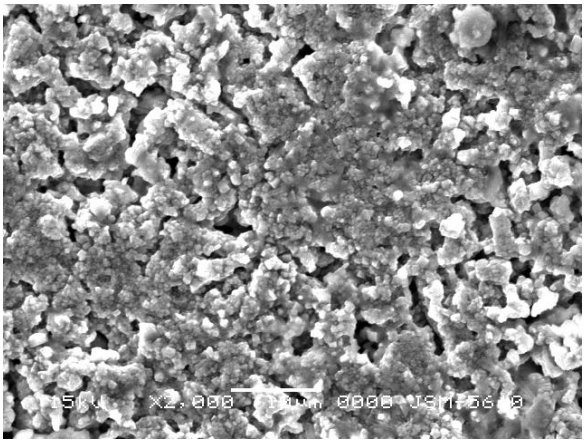

Fig. 4.10 SEM of $Li_{1.3}Al_{0.3}Y_{0.3-x}Ti_{1.7}(PO_4)_3$ for x= 0.15 sample at 2000 X magnification

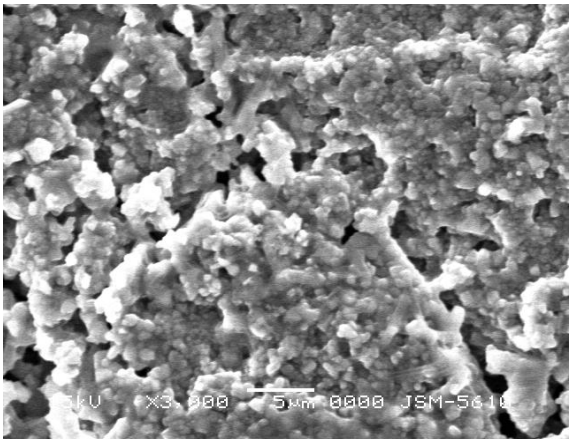

Fig. 4.11 SEM of $Li_{1.3}Al_{0.3}Y_{0.3-x}Ti_{1.7}(PO_4)_3$ for x= 0.15 sample at 3000X magnification

It can be seen from the SEM pictures of the two samples S1 (x = 0.01) and S6 (x = 0.15) of the LAYTP series that grains are well formed. The interface between two grains in both cases is seen. With an increase in yttrium content, bridging and linkages between the grains increases as shown in Fig**.** 4.11. Pores and gaps are clearly visible indicating deformations.

4.3.2 SEM of LAGTP series

The SEM pictures of two samples of LAGTP series are presented below (Figs. 4.12 to 4.15). The formation of grains is clearly visible in both the samples. From Fig**.** 4.13 it is noticed that small granules of irregular shape aggregate to form grains. Gaps between grain-aggregates give limited connection between grains.

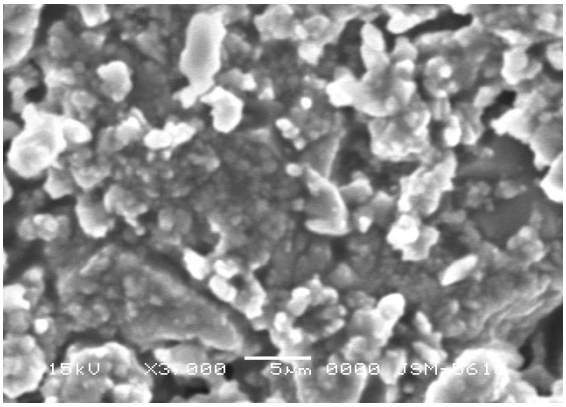

Fig. 4.12 SEM of $Li_{1.3}Al_{0.3}Ga_{0.3-x}Ti_{1.7}(PO_4)_3$ series for x= 0.01 sample at 3000 X magnification

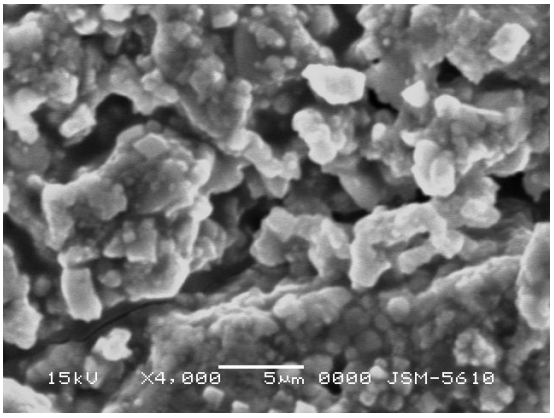

Fig. 4.13 SEM of $Li_{1.3}Al_{0.3}Ga_{0.3-x}Ti_{1.7}(PO_4)_3$ series for x= 0.01 sample at 4000 X magnification

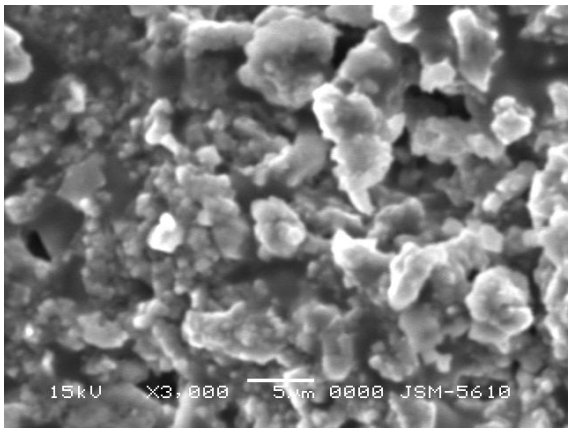

Fig. 4.14 SEM of $Li_{1.3}Al_{0.3}Ga_{0.3-x}Ti_{1.7}(PO_4)_3$ series for x= 0.05 sample at 3000X magnification

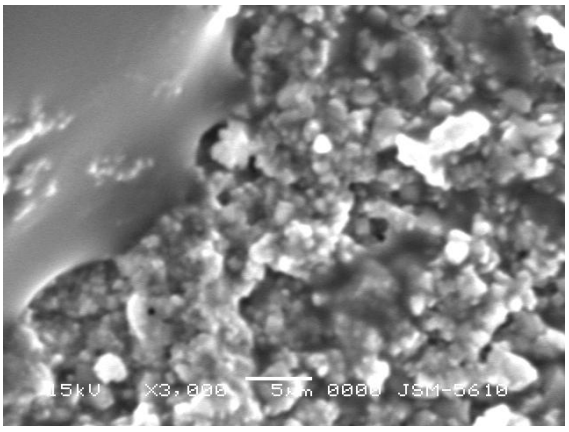

Fig. 4.15 SEM of $Li_{1.3}Al_{0.3}Ga_{0.3-x}Ti_{1.7}(PO_4)_3$ series for x= 0.07 sample at 3000X magnification

There is some linking and contacts especially when the phases between the grains, melt when amount of gallium is increased which are glassy melt phases.

4.3.3 SEM of LASTP series

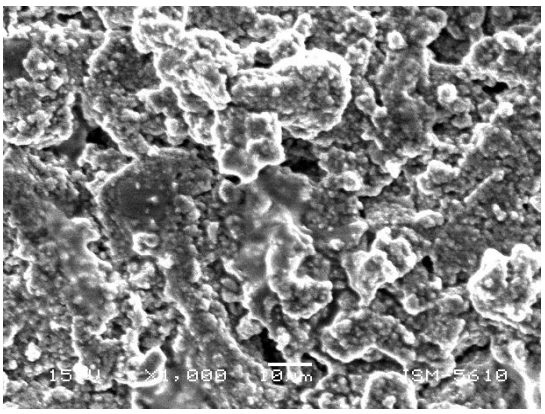

Fig. 4.16 SEM of $Li_{1.3}Al_{0.3}Sc_{0.3-x}Ti_{1.7}(PO_4)_3$ series for x= 0.01 sample at 1000X magnification

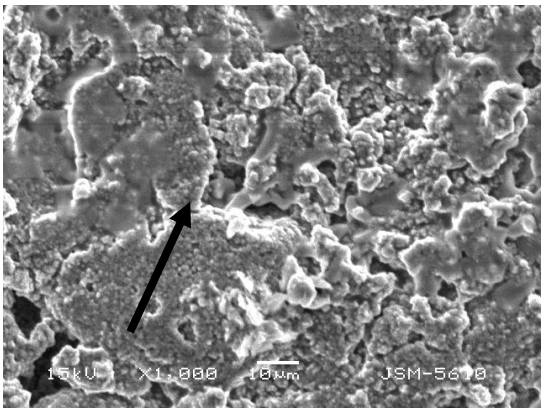

Fig. 4.17 SEM of $Li_{1.3}Al_{0.3}Sc_{0.3-x}Ti_{1.7}(PO_4)_3$ series for x= 0.03 sample at 1000X magnification

At 1000 X magnification, the formation of grains is visible but linkages and contacts between the grains when amount of scandium is increased are not very clearly visible (Figs. 4.16 and 4.17). At some of the places the glassy (melted) phases (especially in Figs**.** 4.17 and 4.19) indicated by black arrows is visible on the surface.

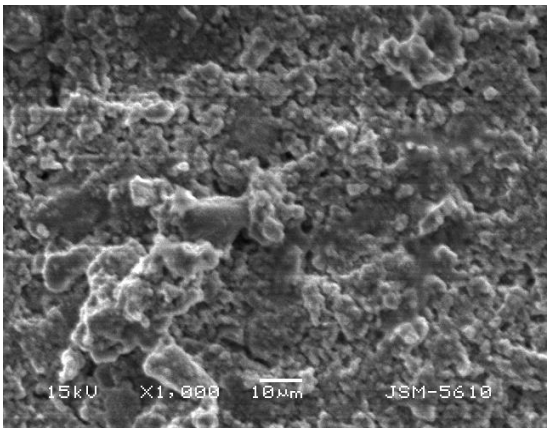

Fig. 4.18 SEM of $Li_{1.3}Al_{0.3}Sc_{0.3-x}Ti_{1.7}(PO_4)_3$ series for x= 0.05 sample at 1000X magnification

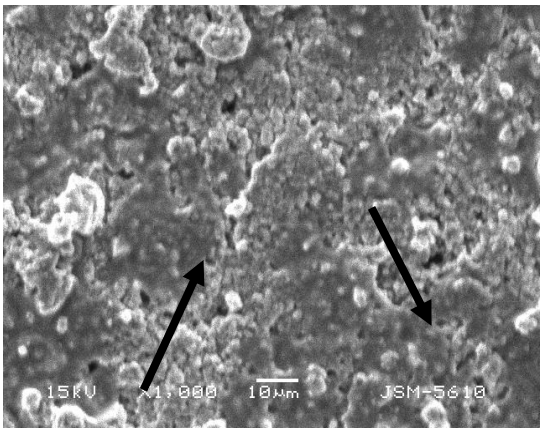

Fig. 4.19 SEM of $Li_{1.3}Al_{0.3}Sc_{0.3-x}Ti_{1.7}(PO_4)_3$ series for x= 0.07 sample at 1000X magnification

White marks at some places in the sample indicate the interaction with the electron beam due to uneven surface morphology. Fig. 4.18 indicates the formation of small grains at 1000X while fig. 4.19 indicates the surface melting of phases when scandium is high in the system.

4.4. Transport Number Measurements

The transport number measurements were done using the DC polarization method. From the results shown in table 4.4.1 below, the LAGTP series has higher Li^+ transport compared to its parent system. The transport numbers decrease in general as dopant concentration increase, however for samples of LASTP series, the transport number is almost the same for all samples. While the samples with least dopant concentrations (and correspondingly higher transport numbers) indicate an ionic character the samples with higher dopants and lesser values of transport numbers indicate a mixed ion electronic conductivity. That is, electron conductivity is also present in them. The presence of blocking impurities like YPO_4, TiO_2, TiP_2O_7 and $LiTiO_5$ in the LAYTP series suggest the blocking of Li^+ ions at the M1 and M2 sites. It has been suggested that [18, 24, 31] presence of such large cations (Y (0.93 Å)) near the tetrahedral and octahedral sites block Li^+ ions from the bottlenecks. This is a contributing reason for less ionic conductivity in doped samples.

Table 4.4.1

Transport numbers for different samples

Sample series		T_{Li} %
LTP		83%
LATP		89%
LAYTP series:	Sample S1 (x = 0.01)	85%
	Sample S2 (x = 0.03)	82%
	Sample S3 (x = 0.05)	79%
	Sample S4 (x = 0.07)	76%
	Sample S5 (x = 0.10)	78%
	Sample S6 (x = 0.15)	77%
LAGTP series:	Sample G1 (x = 0.01)	90%
	Sample G2 (x = 0.03)	87%
	Sample G3 (x = 0.05)	82%
	Sample G4 (x = 0.07)	81%
LASTP series:	Sample N1 (x = 0.01)	76%
	Sample N2 (x = 0.03)	74%
	Sample N3 (x = 0.05)	75%
	Sample N4 (x = 0.07)	75%

Aono *et al.* [4, 30] have suggested formation of mixed phases when yttrium and scandium are doped in the LTP system. Lithium forms phases apart from the main LTP phase. Such phases generally are insulating in nature. They do not contribute in Li^+ transport across. The presence of amorphous phases like $AlPO_4$, $GaPO_4$, $ScPO_4$, TiO_2 etc at grain boundary have been suggested in a number of studies [17, 20, 32]. In fact Wong *et al.* [33] have suggested three different phases of $AlPO_4$ are formed at increasing temperatures in LATP NASICON compound. Berlinite and Crystoballite phases are formed below 1000 ˚C while Tridimite is formed above 1000 ˚C. They are irreversible phases. That is, once Al is locked into these phases, it cannot contribute to Li^+ conductivity in the system. Thus locking of Al is an indirect factor which also contributes in lesser amount of Li^+ conductivity [5].

4.5 Electron Dispersive Spectroscopy Measurements

4.5.1 EDS of LAYTP series

The energy dispersive spectroscopy is performed to study the elemental composition on the surface of the solid specimen. We have performed the EDS to ascertain the percentage and amounts of constituents in our different series. The electron beam was focused on a small 500 micron area (see Fig. 4.20). These results are presented in Figs. 4.20 to 4.23 and Table 4.5.1. From the values it is clear that a very small amount of yttrium is present in samples due to very less percentage of doping. Other impurities like potassium and silicon were also detected from the surface of one sample. Even though yttrium is present in small quantity – it is known to get segregated towards the grain boundary and affect the Li^+ conductivity at periphery of grains [34, 35]. In fact Yan *et al.* [36] have concluded from their extensive studies on heavily doped yttria on ceria that yttrium forms nano-domains at the grain boundary which gives rise to space charge zones in the local area and gives rise to blocking effects. Many others workers [34-40] have found increasing amount of grain boundary thickness and increased yttrium concentration profiles when doping level of yttrium was increased. Some have also found Mott Schottky model of potential barrier to support their

space charge concept. From the above results, it can be said that presence of other impurities might also cause blocking of Li^+ within grains and grain boundaries.

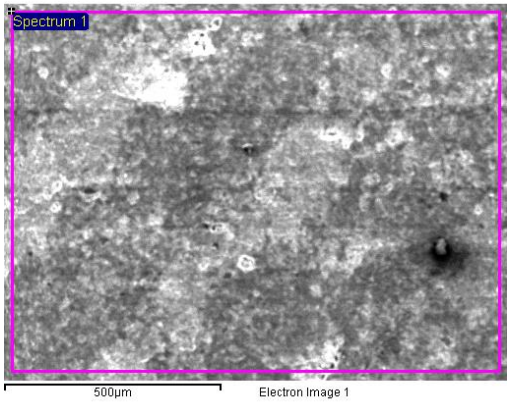

Fig. 4.20 Focus area for EDS analysis for $Li_{1.3}Al_{0.3-x}Y_xTi_{1.7}(PO_4)_3$ series for x=0.01 sample

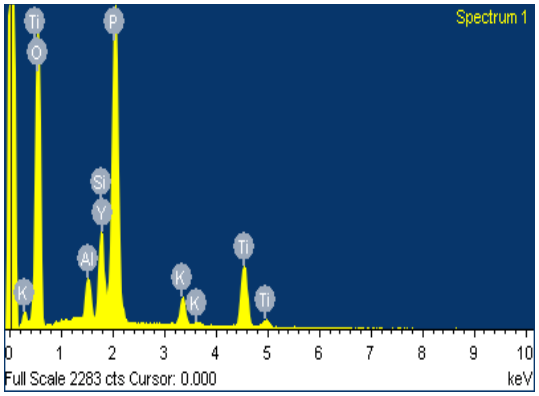

Fig. 4.21 EDS spectrogram for $Li_{1.3}Al_{0.3-x}Y_xTi_{1.7}(PO_4)_3$ series for x=0.01 sample

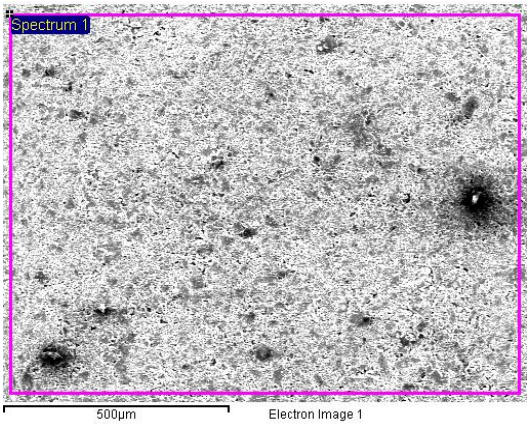

Fig. 4.22 Focus area for EDS analysis for $Li_{1.3}Al_{0.3-x}Y_xTi_{1.7}(PO_4)_3$ system for x=0.15 sample

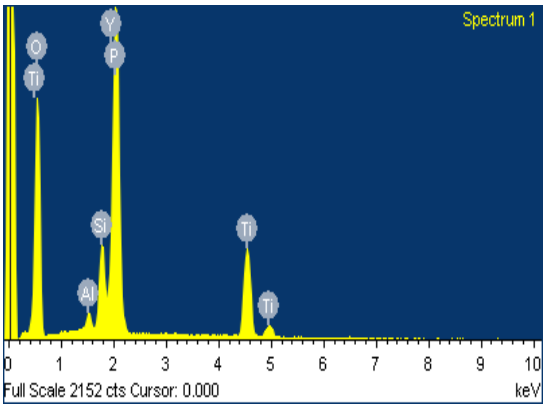

Fig. 4.23 EDS spectrogram for $Li_{1.3}Al_{0.3-x}Y_xTi_{1.7}(PO_4)_3$ system for x=0.15 sample

Table 4.5.1
EDS results of samples S1 (x = 0.01) and S6 (x = 0.15)

Sample S1 (x = 0.01)			Sample S6 (x = 0.15)		
Element	**Weight%**	**Atomic%**	**Element**	**Weight%**	**Atomic%**
O *K*	59.36	75.31	O *K*	54.75	73.15
Al *K*	2.22	1.67	Al *K*	0.83	0.66
Si *K*	4.72	3.41	Si *K*	4.43	3.37
P *K*	21.3	13.96	P *K*	21.93	15.13
K *K*	1.84	1.36	Ti *K*	16.23	7.24
Ti *K*	10.56	4.48	Y *L*	1.84	0.44
Y *L*	0.79	0.18			
Total	100	100	Total	100	100

K = K shell ***L*** = L shell

4.5.2 EDS of LAGTP series

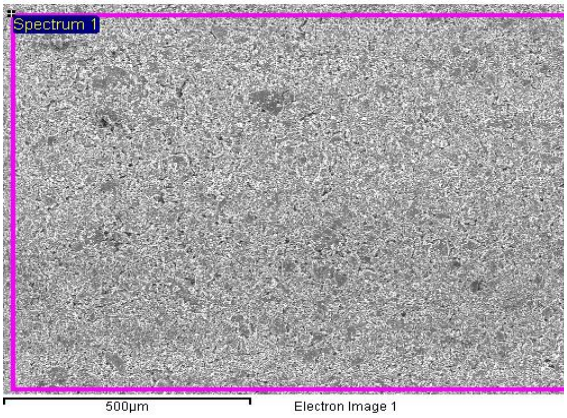

Fig. 4.24 Focus area for EDS analysis of $Li_{1.3}Al_{0.3-x}Ga_xTi_{1.7}(PO_4)_3$ system for x=0.01 sample

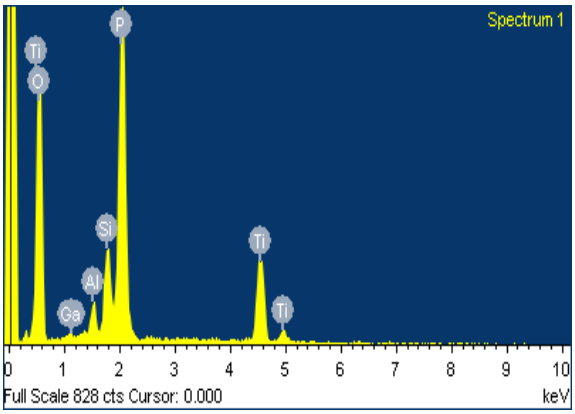

Fig. 4.25 EDS spectrogram of $Li_{1.3}Al_{0.3-x}Ga_xTi_{1.7}(PO_4)_3$ system for x=0.01 sample

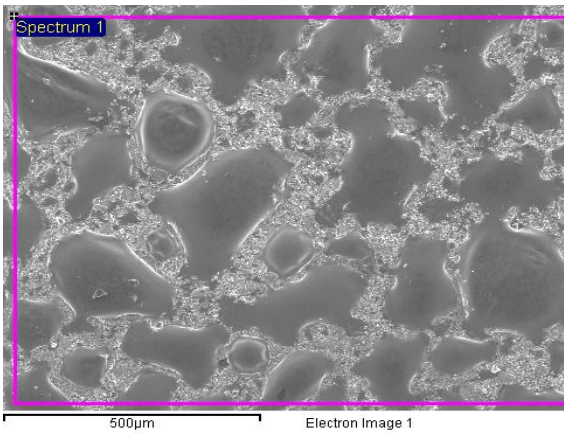

Fig. 4.26 Focus area for EDS analysis of $Li_{1.3}Al_{0.3-x}Ga_xTi_{1.7}(PO_4)_3$ system for x=0.07 sample

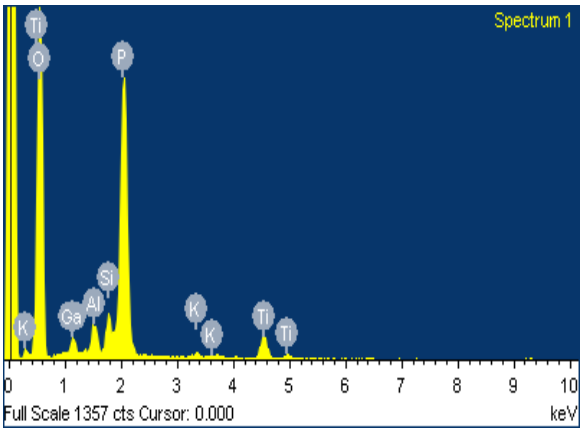

Fig. 4.27 EDS spectrogram of $Li_{1.3}Al_{0.3-x}Ga_xTi_{1.7}(PO_4)_3$ system for x=0.07 sample

EDS was performed on gallium doped LATP compound for samples G1 and G4. The results (focus area and spectrograms) are enlisted in Figs. 4.24 to 4.27.

The results of the LAGTP series for two samples G1 and G4 are tabulated in Table 4.5.2. It shows a very small amount of gallium in the sample G1. The amount of gallium increases for sample G4. It is clear from a number of studies that as gallium increases in the system, it starts to segregate towards grain boundary [19, 20, 30, 41-43]. It also improves the sinterability of the material.

Table 4.5.2
EDS results of sample G1 (x = 0.01) and G4 (x = 0.07)

Sample G1 (x = 0.01)			Sample G4 (x = 0.07)		
Element	**Weight%**	**Atomic%**	**Element**	**Weight%**	**Atomic%**
O *K*	56.78	74.08	**O *K***	64.59	79.28
Al *K*	1.59	1.23	**Al *K***	2.01	1.46
Si *K*	4.42	3.28	**Si *K***	2.12	1.48
P *K*	21.86	14.73	**P *K***	23.47	14.88
Ti *K*	15.29	6.66	**K *K***	0.42	0.21
Ga L	0.05	0.01	**Ti *K***	4.7	1.93
			Ga *L*	2.69	0.76
Total	100		**Total**	100	

K = K shell ***L*** = L shell

Gallium has low melting point. It is a main group element in the periodic table and has a **s**-orbital as valence shell. It forms oxides readily and can easily settle on the surface where oxygen is more easily available. It also forms stable phosphates ($GaPO_4$) which easily get segregated towards grain boundary.

4.5.3 EDS of LASTP series

EDS results of scandium doped LATP system for two samples N1 and N4 are presented below (Figs.4.28 to 4.31 and Table 4.5.3). The proportion of scandium is varied from 0.01 to 0.07.

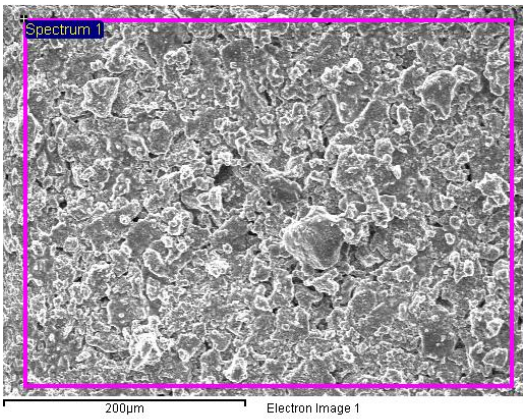

Fig. 4.28 Focus area for EDS analysis of $Li_{1.3}Al_{0.3-x}Sc_xTi_{1.7}(PO_4)_3$ system for x= 0.01 sample

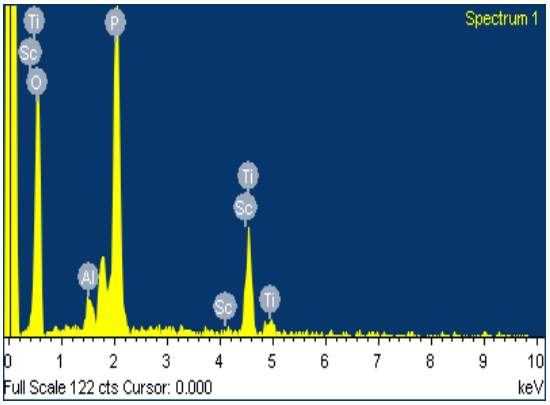

Fig. 4.29 EDS spectrogram of $Li_{1.3}Al_{0.3-x}Sc_xTi_{1.7}(PO_4)_3$ system for x = 0.01 sample

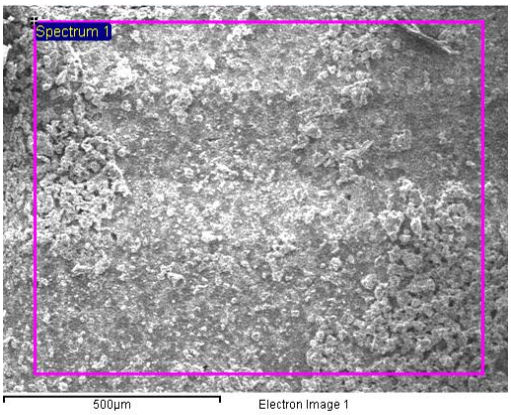

Fig. 4.30 Focus area for EDS analysis of $Li_{1.3}Al_{0.3-x}Sc_xTi_{1.7}(PO_4)_3$ for x=0.07 sample

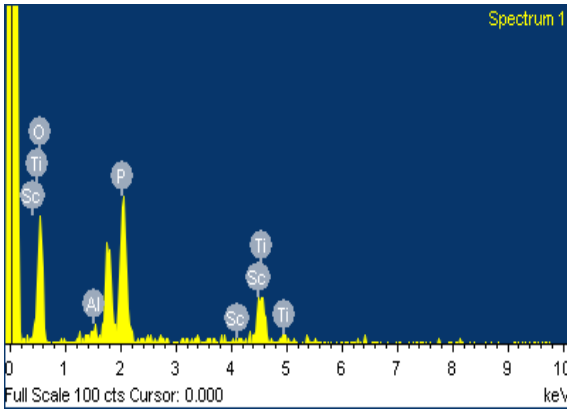

Fig. 4.31 EDS spectrogram of $Li_{1.3}Al_{0.3-x}Sc_xTi_{1.7}(PO_4)_3$ for x=0.07 sample

There is only a marginal increase in the amount of scandium on the surface of the samples. The scandium forms compounds like $ScPO_4$ which segregate towards grain boundary. This has been ascribed in a number of studies in which the profile of scandium increases at grain boundary core when scandium doping was increased [34] in Sc-doped ion conducting system.

Table 4.5.3
EDS results of sample N1 (x = 0.01) and N4 (x = 0.07)

Sample N1 (x = 0.01)			**Sample N4 (x = 0.07)**		
Element	**Weight%**	**Atomic%**	**Element**	**Weight%**	**Atomic%**
O *K*	57.89	75.49	**O *K***	58.86	76.33
Al *K*	2.06	1.59	**Al *K***	2.26	1.74
P *K*	22.94	15.46	**P *K***	21.45	14.37
Sc *K*	0.3	0.14	**Sc *K***	0.41	0.19
Ti *K*	16.81	7.32	**Ti *K***	17.02	7.37
Total	100		**Total**	100	

K = K shell ***L*** = L shell

In the present case also, $ScPO_4$ is formed in an increasing amount as sc-doping increases. This scandium gets accumulated at grain boundary. Thus we find that dopants increase proportionately as their concentration in the system was increased.

References:

[1] JCPDS Card No. 79-1640

[2] JCPDS Card No. 38-1468

[3] R. Ramaraghavulu, S. Budhhudu, Ceramic International 37 (2011) 3651

[4] H. Aono, E. Sugimoto, Y. Sadaoka, N. Imanaka, G. Adachi, Solid State Ionics, 40-41(1990) 38

[5] P. Maldonado-Manso, M.A.G. Aranda, S. Bruque, J. Sanz, E.R. Losilla, Solid State Ionics 176 (2005) 1613

[6] J. Fu, Solid State Ionics 96 (1997) 195

[7] M.A. Paris, A.M. Juarez, J.M. Rojo, J. Sanz, J. Phys. Condens. Matter 8 (1996) 5355

[8] E.R. Losilla, M.A.G. Aranda, S. Bruque, M.A. Paris, J. Sanz, A.R. West, Chem. Mater. 10 (1998) 665

[9] M. Forsyth, S. Wong, K. M. Nairn, A.S. Best, P.J. Newman, D.R. MacFarlane, Solid State Ionics 124(1999) 213

[10] A.S. Best, M. Forsyth, D.R. MacFarlane, Solid State Ionics 136-137 **(**2000) 339

[11] S. Wong, P.J. Newman, A.S. Best, K.M. Nairn, D.R. MacFarlane, M. Forsyth, J. Mater. Chem. 8 (1998) 2199

[12] K. Arbi, S. Mandal, J. M. Rojo, J. Sanz, Chem. Mater. 14 (2002) 1091

[13] F. Cherkaoui, J.C. Viala, C. Delmas, P. Hagenmuller, Solid State Ionics 18-19 **(**1986) 333

[14] A.F. Orliukas, T. Salkus, A. Kezionis, A. Dindune, Z. Kanepe, J. Ronis, V. Venckute, V. Kazlauskiene, J. Miskinis, A. Lukauskas, Solid State Ionics 225(2012) 620

[15] T. Salkus, E. Kazakevicius, A. Kezionis, A. Dindune, Z. Kanepe, J. Ronis, J. Emery, A. Boulant, O. Bohnke , A.F. Orliukas, J. Phys: Condens. Matter 21 (2009) 185502

[16] T. Salkus, E. Kazakevicius, A. Kezionis, V. Kazlauskiene, J. Miskinis, A. Dindune, Z. Kanepe, J. Ronis, M. Dudek, M. Bucko, J.R. Dygas, W. Bogusz, A.F. Orliukas, Ionics 16 **(**2011) 631

[17] E. Kazakevicius, T. Salkus, A. Selskis, A. Selskiene, A. Dindune, Z. Kanepe, J. Ronis, J. Miskinis, V. Kazlauskiene, V. Venckute, A. Kezionis, A.F. Orliukas, Solid State Ionics 188 **(**2012) 73

[18] T. Salkus, M. Barre, A. Kezionis, E. Kazakevicius, O. Bohnke, A. Selskiene, A.F. Orliukas, Solid State Ionics 225 (2012) 615

[19] J. Fu, J. Mat. Sci. 33 (1998) 1549

[20] C.K.K. Reddy, B.R. Ravuri, V. K. Reddy, K.V. Rao, Phase Transitions 85 (2012) 218

[21] H. Yoshida, K. Miura, J. Fujita, T. Inagaki, J. Am, Ceram. Soc. 82 (1999) 219

[22] X. Guo, W. Sigle, J. Fleig, J. Maier, Solid State Ionics 154-155 (2002) 555

[23] P.F. Yan, T. Mori, A. Suzuki, Y.Y. Wu, G.J. Auchterlonie, J. Zou, J. Drennan, Solid State Ionics 222-223 (2012) 31

[24] R.O. Fuentes, F.M. Figuieredo, F.M.B. Marques, J.I. Franco, Solid State Ionics 140 **(**2001) 173

[25] Q. Wang, O. Varghese, C.A. Grimes, E.C. Dickey, Solid State Ionics 178 **(**2007) 187

[26] M.A. Subramanian, R. Subramanian, A. Clearfield, Solid State Ionics 18-19 (1986) 562

[27] K. Ado, Y. Saito, T. Asai, H. Kageyama, O. Nakamura, Solid State Ionics 53-56 (1992) 723

[28] F.E. Mouahid, M. Bettach, M. Zahir, P. Maldonado-Manso, S. Bruque, E.R. Losilla, M.A.G. Aranda, J. Chem. Mater. 10 (2000) 2748

[29] Y. Saito, T. Asai, K. Ado, H. Kageyama, O. Nakamura, Solid State Ionics 40-41 (1990) 34

[30] H. Aono, E. Sugimoto, Y. Sadaoka, N. Imanaka, G. Adachi, J. Electrochem. Soc. 137 (1990) 1023

[31] I.Y Pinus, A.V. Khoroshilov, K.S. Gavrichev, V.P. Tarasov, A.B. Yaroslavtsev, Solid State Ionics 212 (2012) 112

[32] G.G. Amatucci, A. Safari, F.K. Skokoohi, B.J. Wilkens, Solid State Ionics 60 (1993) 357

[33] S. Wong, P.J. Newman, A.S. Best, K.M. Nairn, D.R. MacFarlane, M. Forsyth. J. Mater. Chem. 8 (1998) 2199

[34] M. Shirpour, B. Rahmati, W. Sigle, P.A. van Aken, R. Merkle, J Maier, J. Phys. Chem C. 116 (2012) 2453

[35] M. Shirpour, R. Merkle, C.T. Lin, J. Maier, Phys. Chem. Chem. Phys. 14 (2012) 730

[36] F. Krok, Solid State Ionics, 124 (1987) 24

[37] H. Maekawa, K. Kawata, Y.P. Xiong, N. Sakai, H. Yokokawa, Solid State Ionics 180 (2009) 314

[38] C.T. Chen, C.E. Danel, S. Kim, J. Mater Chem. 21 (2011) 5435

[39] X Guo, R Waser, Solid State Ionics 173 (2004) 63

[40] F. Iguchi, N. Sata, H. Yugami, J. Mater. Chem. 20 (2010) 6265

[41] H. Yoshida, K. Miura, J. Fujita, T. Inagaki, J. Am. Ceram. Soc. 82 (1999) 219

[42] S. Istomin, E.V. Antipov, Yu S. Fedotov, S.I. Bredikhin, N.V. Lyskov, S. Shafeie, G. Svensson, Y. Liu, Z. Shen, J. Solid State Electrochem. (2013) *DOI 10.1007/s10008-013-2190-4.*

[43] D.H. Kothari, D. K. Kanchan, Ionics 21 (2014) 1287

****